

Deep ice layer formation in an alpine snowpack: monitoring and modelling

Louis Quéno¹, Charles Fierz¹, Alec van Herwijnen¹, Dylan Longridge¹, and Nander Wever²

¹WSL Institute for Snow and Avalanche Research SLF, Davos, Switzerland

²Department of Atmospheric and Oceanic Sciences, University of Colorado Boulder, Boulder, CO, USA

Correspondence: Louis Quéno (queno@slf.ch)

Abstract. Ice layers may form deep in the snowpack due to preferential water flow, with impacts on the snowpack mechanical, hydrological and thermodynamical properties. This detailed study at a high-altitude alpine site aims at monitoring their formation and evolution thanks to the combined use of a comprehensive observation dataset at daily frequency and state-of-the-art snow-cover modelling with improved ice formation representation. In particular, daily SnowMicroPen penetration resistance profiles enabled to better identify ice layer temporal and spatial heterogeneity when associated with traditional snowpack profiles and measurements, while upward-looking ground penetrating radar measurements enabled to detect the water front and better describe the snowpack wetting when associated with lysimeter runoff measurements. A new ice reservoir was implemented in the one-dimensional SNOWPACK model, which enabled to successfully represent the formation of some ice layers when using Richards equation and preferential flow domain parameterization, during winter 2017. The simulation of unobserved melt-freeze crusts was also reduced. These improved results were confirmed over 17 winters. Detailed snowpack simulations with snow microstructure representation, associated with high-resolution comprehensive observation dataset were shown relevant for studying and modelling such complex phenomena, despite limitations inherent to 1D modelling.

1 Introduction

The presence of ice layers in a snowpack may impact its mechanical, hydrological and thermodynamical properties. Monitoring the formation and evolution of ice layers is thus crucial in many research fields. Because of their low permeability (Albert and Perron Jr., 2000), ice layers may increase the liquid water storage of the snowpack, which can substantially affect the snowpack runoff (Singh et al., 1999). On the contrary, near-surface ice layers in Greenland were shown to prevent access to deeper firn layers, thus reducing meltwater storage in the firn and enhancing ice sheet mass loss (Machguth et al., 2016). The stability of a mountainous snowpack may also be affected, with a possible increased faceting of the microstructure close to ice or crusts (Jamieson, 2006; Hammonds et al., 2015; Hammonds and Baker, 2016). Moreover, retrieval algorithms for water equivalent of snow cover and snow depth from passive microwave emissions are sensitive to the presence of ice layers (Rees et al., 2010; Roy et al., 2016). Better knowledge about their formation could help the assimilation of such data in detailed snow-cover models (Larue et al., 2018).

Ice forms in the snowpack can have different origins (Fierz et al., 2009). They can either form at the surface, because of
25 freezing rain (Quéno et al., 2018) or firnspiegel formation process due to radiative cooling (Ozeki and Akitaya, 1998), or they
can form within the snowpack, through percolation of rain or meltwater reaching subfreezing snow (Pfeffer and Humphrey,
1998). The present study focuses on the latter case. As opposed to matrix water flow, leading to a homogeneous progression
of the wetting front, preferential water flow occurs through flow fingering (e.g. Schneebeli, 1995), transporting liquid water to
deeper regions of the snowpack where the cold content is sufficient to refreeze it (e.g. Marsh, 2006). Preferential flow occurs
30 in the snowpack due to its microstructural heterogeneity (density, grain size and shape) at layer transitions (Katsushima et al.,
2013), which may trigger flow fingering or form hydraulic barriers (i.e. capillary or permeability barriers) where water ponds
and may subsequently refreeze. Hydraulic barriers may also divert water flow and lead to lateral flow along slopes (Eiriksson
et al., 2013; Webb et al., 2018a). Knowledge about water percolation in snow, and particularly preferential flow, has recently
made great progress in terms of process understanding and numerical simulation. Using dye tracer and liquid water content
35 (LWC) measurements, Avanzi et al. (2016) observed preferential flow and water ponding at capillary barriers for various layer
transition characteristics and water input. X-ray microtomography was also used to observe wet-snow metamorphism under
preferential flow (Avanzi et al., 2017). Magnetic Resonance Imaging observations of finger flow and lateral flow emphasized
that even small differences in snow properties may form capillary barriers in dry snow (Katsushima et al., 2018, 2020). At larger
scale, the effect of preferential flow on the snowpack runoff was assessed, through measurements of the heterogeneity of water
40 discharge (Yamaguchi et al., 2018; Webb et al., 2018b), or under rain-on-snow conditions (Würzer et al., 2017; Juras et al.,
2017). The new insights from measurement campaigns enabled the development of multi-dimensional models accounting for
preferential flow in the snowpack (Hirashima et al., 2014, 2017, 2019; Leroux and Pomeroy, 2017, 2019). They also enabled
progress in the representation of water transport in one-dimensional (1D) models. Richards equation was implemented in
detailed snow-cover models like SNOWPACK (Wever et al., 2014) and Crocus (D'Amboise et al., 2017), as an improvement
45 over the more simplistic bucket parameterization, enabling a more realistic representation of water transport in snow with
respect to snow microstructure. Based on recent studies relating preferential flow to snow properties (Katsushima et al., 2013;
Hirashima et al., 2014; Yamaguchi et al., 2012), with analogies to preferential flow in soils (DiCarlo, 2007, 2013), Wever et al.
(2016) developed an original 1D parameterization of preferential flow in SNOWPACK through a dual-domain implementation
separating matrix flow and preferential flow, both solved with Richards equation.

50 The representation of ice layer formation in snow-cover models remains very challenging because it depends on an accurate
description of the snow microstructure and water transport. Currently, most snow-cover models don't take into account the
processes of ice layer formation. Quéno et al. (2018) recently modelled ice formation on the snowpack surface due to freezing
precipitation in the detailed snow-cover model Crocus. Wever et al. (2016) included for the first time in a detailed snow-cover
model the process of deep ice layer formation due to preferential water flow. Using the dual-domain implementation for water
55 percolation in a sub-freezing snowpack, they investigated ice layer formation at an alpine site, comparing manual snow profiles
recorded every two weeks over 16 winter seasons with SNOWPACK simulations. Nevertheless, many research gaps remain
open about deep ice layer formation in the snowpack. In particular, the present study aims at answering the following questions:

- Can daily SnowMicroPen measurements improve the monitoring of ice layers in natural snowpacks over traditional snowpack profiling?
- 60 – How well can 1D snow-cover models represent a multi-dimensional process like ice formation due to preferential flow?
- Can spatially discontinuous ice lenses be parameterized in a 1D snow-cover model?
- Can we provide useful information on ice layer origin and evolution in alpine snowpacks for various applications, based on observations and simulations?

To address these research questions, we bring several novelties in a detailed study pushing forward the investigation of Wever et al. (2016). First, a comprehensive observation dataset was gathered at the same research site, in order to better determine the evolution of the snowpack and identify the formation of deep ice layers in natural conditions at a high-altitude alpine site. The originality of this dataset comes from the opportunity to monitor ice formation in natural alpine conditions during a whole winter season at daily resolution, even though the present study does not include detailed observations of preferential water flow paths. This dataset is then used for a detailed assessment of the preferential flow representation in SNOWPACK, bringing 70 complementary insights to Wever et al. (2016) and Würzer et al. (2017). As a result, we introduce a new parameterization to improve the simulation of discontinuous deep ice formation in the SNOWPACK model.

The paper is organized as follows. Section 2 describes the study site, the observation dataset, the snowpack simulation configuration and new methods. Section 3 details the results with insights on water percolation and ice layer formation from both the observation dataset and the simulations. Their benefits and limitations are discussed in Sect. 4.

75 **2 Data and methods**

2.1 Observation dataset

The site of study is the Weissfluhjoch (WFJ) measurement site, a research field dedicated to snowpack investigations, located at an elevation of 2536 m.a.s.l. above Davos in the Eastern Swiss Alps (Marty and Meister, 2012). For comparison to simulations, we use a comprehensive observation dataset collected during winter 2017. Figure 1 indicates the location of the measurements 80 in the research field. Traditional snowpack profiles were performed during the entire season every week (or every two weeks at the beginning and the end of the season) along three corridors, moving continuously along each corridor and turning into the next one once the end of the previous one was reached. These profiles were carried out following the recommendations of Fierz et al. (2009) and gather observations of the grain shape, grain size, layer thickness, hand hardness index and wetness through visual and manual assessment, as well as measurements of snow depth (HS), water equivalent of snow cover (SWE), 85 snow density, snow temperature, snow hardness (Swiss ramsonde), and liquid water content with a Denoth device (Denoth, 1989). Continuous melt-freeze crusts (MFCr) and ice layers (IFil) were identified in the snow profile, while ice lenses were most often noted additionally. There was no measurement of ice layer density, as such measurements in natural conditions remain very challenging (e.g. Watts et al., 2016). Snowpack runoff measurements were provided by a 5 m² lysimeter at 10 min

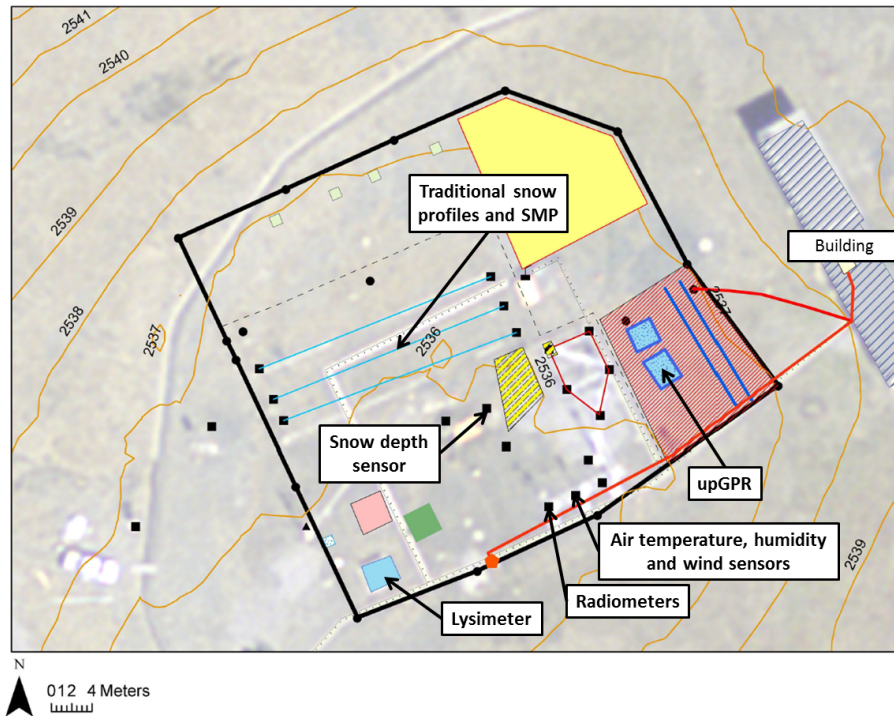


Figure 1. Overview of the WFJ research field, with contour lines in orange and labels indicating the location of the measurements used in this study.

temporal resolution (Wever et al., 2014). Finally, thermistores at a fixed vertical interval of 20 cm provided half-hourly snow
 90 temperature profiles of the snowpack (Fierz, 2011).

An upward-looking ground penetrating radar (upGPR) was also installed on the site (Schmid et al., 2014). The dual frequency
 GPR from IDS (Ingegneria Dei Sistemi, Italy) conducted measurements every 30 minutes and with two different frequencies,
 600 MHz and 1.6 GHz. Every measurement contained 1800 traces with 1024 samples. In order to remove system ringing, a
 hoisting device was installed by Schmid et al. (2014) to move the GPR antennas vertically during a measurement cycle. When
 95 transmitting electromagnetic waves into snow, discontinuities result in reflections, refractions and diffractions. The amount
 of energy reflected at the discontinuity is proportional to the relative change across the discontinuity (Reynolds, 2011). The
 percolated water changes the internal properties of the snow. The boundary between wet and dry snow (called water front
 hereafter) appears as a distinct reflector and can then be determined by semi-automatic picking, similarly to the algorithm
 developed by Schmid et al. (2014) for snow surface picking. The picked two-way travel times of the water front are multiplied
 100 by the wave propagation velocity of 0.23 m ns^{-1} , which is a typical value for snow (Sand and Bruland, 1998; Schmid et al.,
 2014). During winter 2017, the water front could be derived until a technical malfunction on 9 April prevents further analysis.
 Due to the 45° angle of beam spread of the upGPR, the footprint in the snowpack where the water front is derived can measure
 a homogeneous state but not local flow fingers.

In addition, daily measurements of the penetration resistance were performed with a SnowMicroPen (SMP; Schneebeli et al., 1999), in the context of the RHOSSA field campaign (Calonne et al., 2020), launched in winter 2016. The SMP has a tip surface of 19.6 mm². Every day during the winter season, five to seven SMP measurements were performed moving forward by steps of about 40 cm along the corridors, with a 15 cm spacing perpendicular to the direction of the corridor, providing indications about the local spatial heterogeneity of potential ice forms. A limited number of gaps in the daily measurements have to be noted, in particular from 25 March to 27 March and 7 and 8 April in the wetting period.

For longer-term observations of ice layers, we gathered traditional snowpack profiles performed every two weeks during the winter seasons 1999/2000 to 2015/2016.

The comprehensive observation dataset of winter 2017 at WFJ is publicly available (see Code and data availability Section).

2.2 Snowpack simulations

2.2.1 Simulation configuration

SNOWPACK simulations were performed for the WFJ study site in winter 2017. They were initialized with a traditional profile recorded on 3 January 2017, to provide a realistic base of the snowpack with a snow depth of 47 cm. The initialization date was chosen early enough to assess the model ability to simulate the microstructure evolution as well as water percolation, but avoiding early season modelling errors, for example, formation of unobserved basal melt-freeze layers. The simulations were driven by optimal in situ meteorological measurements (Fig. 1) of air temperature and humidity (ventilated sensors), near-surface wind, solar and longwave irradiance (WSL Institute for Snow and Avalanche Research SLF, 2015; Wever et al., 2015). The snowfall input is driven by measured snow depth increments (Wever et al., 2015), enabling direct comparisons to measurements and outcomes of Wever et al. (2016). In addition, for air temperatures above 1.2 °C, undercatch-corrected precipitation gauge measurements are considered as rain.

Three water transport schemes implemented in SNOWPACK were evaluated. First, the bucket approach (BA) is a common method used in snow-cover models (e.g. Bartelt and Lehning, 2002; Vionnet et al., 2012), assuming that water is transported to the next downward layer when the liquid water content exceeds the water holding capacity of a given layer (depending on the ice volumetric content of snow; Coléou and Lesaffre, 1998). Second, the Richards equation (RE) was implemented in SNOWPACK by Wever et al. (2014) to account for capillary effects. These effects are modelled taking into account the water retention curve (van Genuchten, 1980) and the hydraulic conductivity of snow (Mualem, 1976; van Genuchten, 1980; Calonne et al., 2012). Third, a dual-domain approach parameterizing preferential flow and using Richards equation (RE/PF) was recently developed. Water exchanges between the matrix domain and the preferential flow domain are determined according to the water entry pressure head in the matrix layers and the saturation in the preferential flow domain: this implementation is described in details in Wever et al. (2016). The two tuning parameters of this scheme were chosen here accordingly to Wever et al. (2016): the threshold in saturation of the preferential flow domain $\Theta_{th} = 0.08$ and the parameter related to the number of flow paths per square meter $N = 0$. In particular, $N = 0$ implies no refreezing of the preferential flow water (Wever et al., 2016). Similarly to Wever et al. (2016), SNOWPACK simulations were carried out at high vertical resolution, with a layer merging threshold

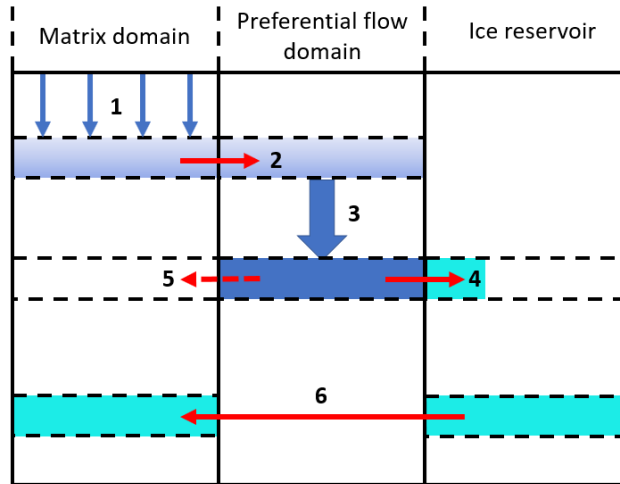


Figure 2. Scheme of the ice reservoir parameterization in SNOWPACK. Blue represents liquid water, cyan represents ice and red arrows represent water or ice transfers to another domain. Steps 1 to 6 are described in the text.

of 0.25 cm and new snow layer initialization of 0.5 cm. High resolution is necessary to permit the formation of very thin high density layers.

2.2.2 Implementation of ice reservoir

- 140 A new parameterization of ice layer formation due to preferential flow was implemented as a complement to the RE/PF scheme. It is summarized in Fig. 2. In the RE/PF scheme, when the saturation in the preferential flow domain exceeds the threshold Θ_{th} , water flows back to the matrix domain. First, a volume of water corresponding to the available freezing capacity is instantly frozen and added uniformly to the ice content of the matrix domain. Ice lenses, to the contrary, may only form locally at the base of the flow fingers. If the threshold is still exceeded then, saturations in both domains are equalized (Wever et al., 2016).
- 145 To better reproduce the formation of continuous ice layers from discontinuous and growing ice lenses, we developed an ice reservoir parameterization. The water normally transferred from the preferential flow domain to the matrix domain that freezes instantly is stored in an ice reservoir (step 4 in Fig. 2), instead of being added to the ice volumetric content of the matrix. The ice reservoir is representative of the volumetric content of ice lenses (i.e. spatially discontinuous ice) in a given layer. The transferred water that does not freeze goes in the matrix domain, i.e. is spread homogeneously (step 5 in Fig. 2).
- 150 Furthermore, the saturation threshold in the PF domain (Wever et al., 2016) was chosen as a simple solution to the inability of Richards equation to model the saturation overshoot present in the tip of flow fingers (DiCarlo, 2007). This simple parameterization can lead to inconsistencies due to the vertical discretization of the simulated snowpack. After water has been transferred to the matrix at the layer corresponding to the finger tip (i.e. where the saturation threshold was exceeded), the highest saturation is then reached more likely at the layer above, where no water transfer occurred, because water percolation from
- 155 this layer to the finger tip layer only occurs at the next time step. Because of that, the water transfer from PF domain to matrix

domain may spread over too many layers, instead of being concentrated in the lowest layer (i.e. the tip of the flow finger). To overcome this issue, the ice reservoir was cumulated in the lowest layer. When the ice volumetric content of the cumulated ice reservoir added to the ice volumetric content and water volumetric content of the associated matrix layer exceeds the corresponding ice density threshold of 700 kg m^{-3} in SNOWPACK, there is enough ice to consider it as horizontally homogeneous: 160 the ice content of the cumulated ice reservoir is then transferred to the associated matrix layer (step 6 in Fig. 2). As long as it is kept in the ice reservoir, the forming ice has no effect on the water transport in the matrix domain that still follows the RE/PF scheme (Wever et al., 2014, 2016). Furthermore, we neglect any impact the ice reservoir, which is interpreted as ice lenses, may have on hydraulic properties (e.g. local hydraulic barrier effect). Simulations with the ice reservoir parameterization are called RE/PF/IceR hereafter.

165 The implementation of the ice reservoir parameterization in the SNOWPACK source code is publicly available (see Code and data availability Section).

3 Results

3.1 Insights from the observation dataset

3.1.1 Overview of the winter season

170 At WFJ, winter 2016/2017 started with a shallow snowpack of approximately 30 cm at the beginning of November, followed by a extended period of calm weather, forming a base layer made of depth hoar crystals (Richter et al., 2019). This layer was covered by new snow at the end of December, and several small snow storms lead to a maximum snow depth of 205 cm on 10 March, i.e. slightly lower than the average maximum snow depth. The snowpack had entirely melted on 14 June. Overall, this winter was characterized by lower snow depth than long-term averages in the region.

175 Figure 3 represents the evolution of grain types within the snowpack as observed in traditional snow profiles. Two layers of particular interest are tracked during the whole winter. Layer 1 corresponds to surface hoar formed at the end of January. This layer is continuously identified as buried surface hoar (as primary or secondary grain) until the end of March, with a grain size substantially larger than the layer above (consisting of rounded grains or faceted crystals), thus constituting a capillary barrier with a classical fine-over-coarse structure (e.g. Avanzi et al., 2016). Ice is observed above this barrier from 28 March, 180 either as a homogeneous layer or as ice lenses mixed with melt forms (red in Fig. 3). Thicknesses between 0.5 cm and 1 cm were reported. The presence of nearby slopes (NNW of the snow profile corridors in Fig. 1) may suggest a water input through lateral flow along the capillary barrier. Simulations (not taking into account lateral flow) may provide complementary insights to determine whether vertical preferential flow was sufficient to form an ice layer. Layer 2 corresponds to surface hoar appearing in mid-February, and forming a capillary barrier once buried. An ice layer is observed at that level in most profiles 185 after 28 March.

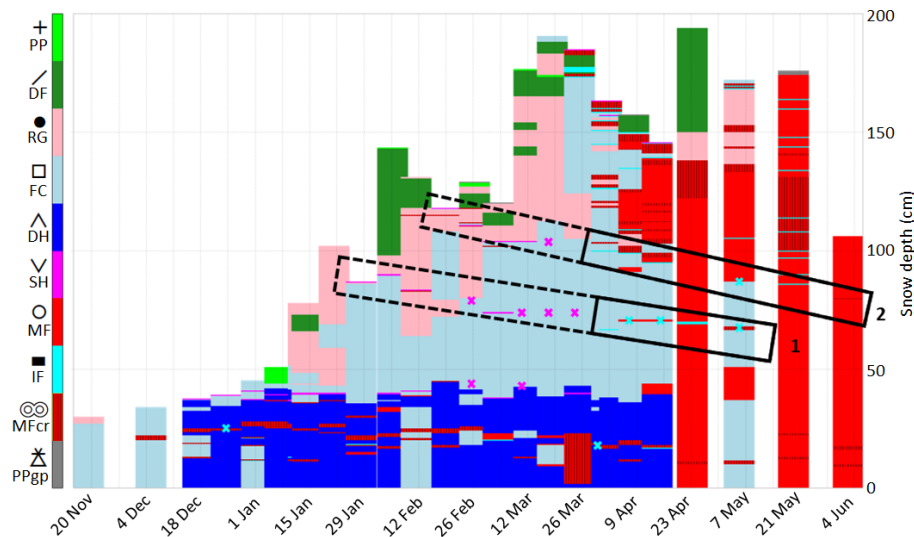


Figure 3. Visual observations of grain shapes at WFJ during winter 2017. Colours, symbols and codes are defined following the grain shape classification of Fierz et al. (2009), fuchsia crosses represent surface hoar as secondary grain shape, cyan crosses represent ice lenses. Rectangles highlight layers 1 and 2, with dashed lines before ice formation and solid lines afterwards.

3.1.2 Water percolation and snowpack runoff

Figure 4 represents lysimeter measurements of the snowpack runoff together with the height of the water front estimated from the upGPR measurements, from 1 March to 15 April, i.e. the transition period from dry to isothermal snowpack. Shown underneath are the snow temperature measurements in the lowest meter of the snowpack, at fixed intervals of 20 cm. The height of water front could only be derived until 8 April due to technical issues. Before 30 March (first dashed line), no snowpack runoff was observed, the water front was always higher than 1 m, and temperatures in the lowest first meter of the snowpack were all below 0°C. Between 30 March and 9 April (second dashed line), the water front remained high (mostly higher than 1 m), a small amount of snowpack runoff was observed (less than 3 kg m⁻² day⁻¹). Snow temperatures gradually increased to reach 0°C by the end of the period in the lowest meter of the snowpack. From 9 April, all temperatures in the lowest meter reach 0°C and snowpack runoff increases. Although after 9 April no more water front estimates were available from the upGPR data, it reached the lowest value (85 cm) on 8 April. The snowpack runoff is yet low compared to the more significant runoff starting in mid-May, as shown in Fig. 5: the first 20 kg m⁻² of total snowpack runoff are reached on 10 April, while the first day with a daily snowpack runoff higher than 10 kg m⁻² day⁻¹ is 13 May.

These measurements give insights in the timing of water percolation in the snowpack. Before 9 April, the bottom of the snowpack was cold and dry while the water front was still mostly above 100 cm. The low snowpack runoff values were thus likely due to preferential flow paths reaching the ground. After 9 April, the lowest meter of the snowpack reaches an isothermal state at 0°C and snowpack runoff increases markedly.

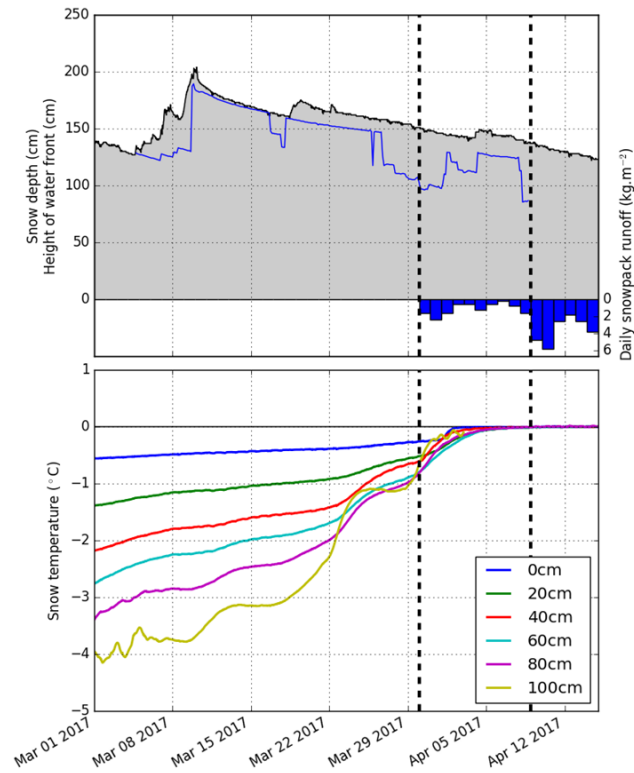


Figure 4. Top: evolution of the snow depth (black line), height of the water front (blue line) and daily snowpack runoff (blue bars), from 1 March 2017 to 15 April 2017 at WFJ. Bottom: measured snow temperatures at different heights above the ground, same period, same location. Dashed lines indicate 30 March and 9 April.

3.1.3 Capillary barriers and ice layers

To study the formation of ice through preferential flow in subfreezing snow, we focus on the lowest meter of the snowpack. In this part, the manual snow profiles enable to identify three main capillary barriers (Fig. 3): the two layers of buried surface hoar where ice forms at the end of March (defined as layers 1 and 2 previously) and the top of the depth hoar base layer, where higher water content is observed in April and May. Layers 1 and 2 are marked by grain size heterogeneity with the overlying layers: on 28 February, 1 mm over 2.5 mm for layer 1, 0.5 mm over 2 mm for layer 2.

Daily SMP measurements enable to more clearly identify the temporal and spatial variability of ice formation. Figure 6 represents the evolution of penetration resistance from 1 February to 19 April, with a scale from 0 N to 2 N to highlight variations in dry snow. The deep MFcr is visible in the middle of a low resistance depth hoar layer, at approximately 20 cm. In February and March, the highest values in the middle of the snowpack correspond to dense layers of faceted crystals (Fig. 3). In March, the buried surface hoar of layer 1 is marked by a lower penetration resistance than the surrounding faceted crystals. Layer 2 exhibits less heterogeneity with surrounding layers. Overall, the penetration resistance increases substantially from the

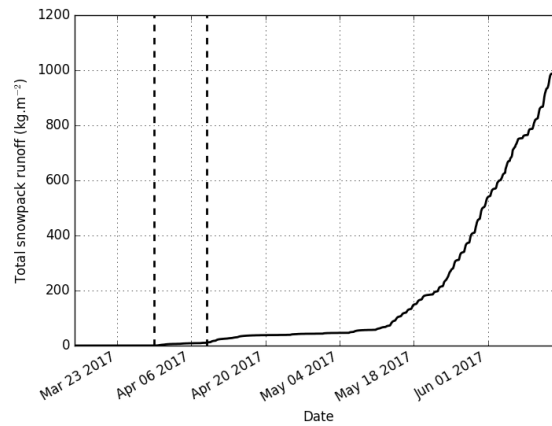


Figure 5. Total snowpack runoff from 15 March 2017 to 15 June 2017 at WFJ. Dashed lines indicate 30 March and 9 April.

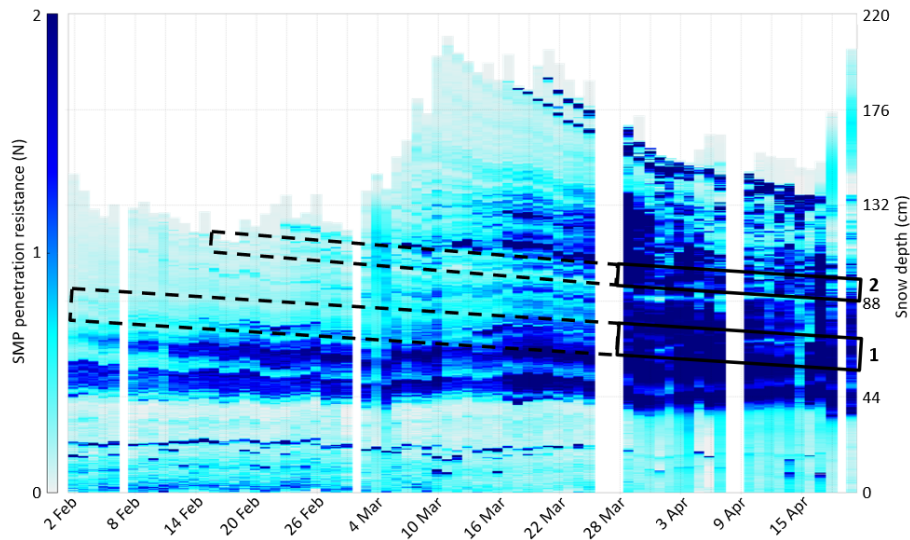


Figure 6. Daily SMP measurements of penetration resistance (mm averaged values) at WFJ from 1 February to 19 April, with one representative profile per day. Values higher than 2 N are shown with the same color. Rectangles highlight the approximate location of layers 1 and 2, with dashed lines before ice formation and solid lines afterwards.

215 end of March on with the progressive wetting, particularly at the top of the snowpack where many melt-freeze crusts form. Figure 7a represents penetration resistances higher than thresholds of 5 N and 10 N, below 100 cm, including all daily SMP measurements. These values were chosen after comparison of matching traditional and SMP profiles, to better highlight crusts and ice forms. Except the deep MFcr mostly visible until the end of March, two high resistance layers can be identified from

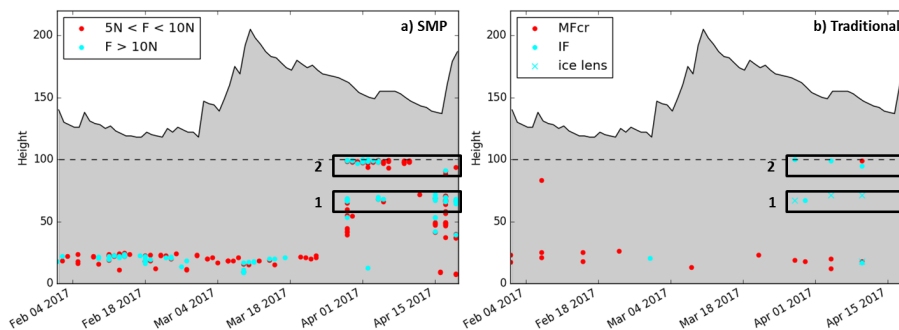


Figure 7. a) Height of SMP penetration resistances between 5 N and 10 N (red) and higher than 10 N (cyan) below 1 m, from 1 February to 19 April at WFJ. b) Visual observations of melt-freeze crusts (MFcr), ice layers (IFil) and ice lenses, same period and location. Daily manual measurements of snow depth in solid black line. Rectangles highlight layers 1 and 2.

29 March: they match the visual identification of ice layers 1 and 2 (Fig. 7b). They can be tracked until mid-April, but are not
 220 present on all SMP profiles.

The penetration resistance measured at these two layers was tracked in the SMP profiles. To identify these layers, all SMP
 profiles were superimposed on the traditional profile observed at the closest date. Penetration resistances were associated to
 observed snow layers given their grain type and hand hardness index. To identify consistent patterns, the SMP profiles of a
 given day were also compared among each other and with those of the previous and next day. The value of SMP penetration
 225 resistance in these layers was then visually picked. Figure 8 shows an example of this procedure for two SMP profiles of 4
 April 2017.

The evolution of the penetration resistance of the two tracked layers is plotted in Fig. 9 from 14 March to 19 April. For
 layer 1, the penetration resistance remains very low (less than 1 N) until 24 March. It corresponds to the observed layer of
 buried surface hoar. On 29 March, all seven SMP measurements show penetration resistance higher than 10 N indicating the
 230 continuous presence of ice. Afterwards, values alternate between low resistance (less than 5 N) and very high resistance (more
 than 10 N), as visible in Fig. 8 on 4 April. This is consistent with the visual observations reporting a layer in which pure
 ice and melt forms are both observed. These observations suggest that water ponding at the capillary barrier did not freeze
 everywhere on the study plot where we performed these measurements. For layer 2, very low penetration resistances are also
 measured until 24 March, corresponding to the observed buried surface hoar. After 29 March, values increase (mostly higher
 235 than 5 N, often more than 10 N), indicating formation of ice. After 9 April, no more high resistances are measured, rather low
 resistances corresponding to a wet layer of melt forms. The evolution of penetration resistances for layer 2 show more temporal
 consistency than layer 1, suggesting that the ice layer disappears totally after 9 April.

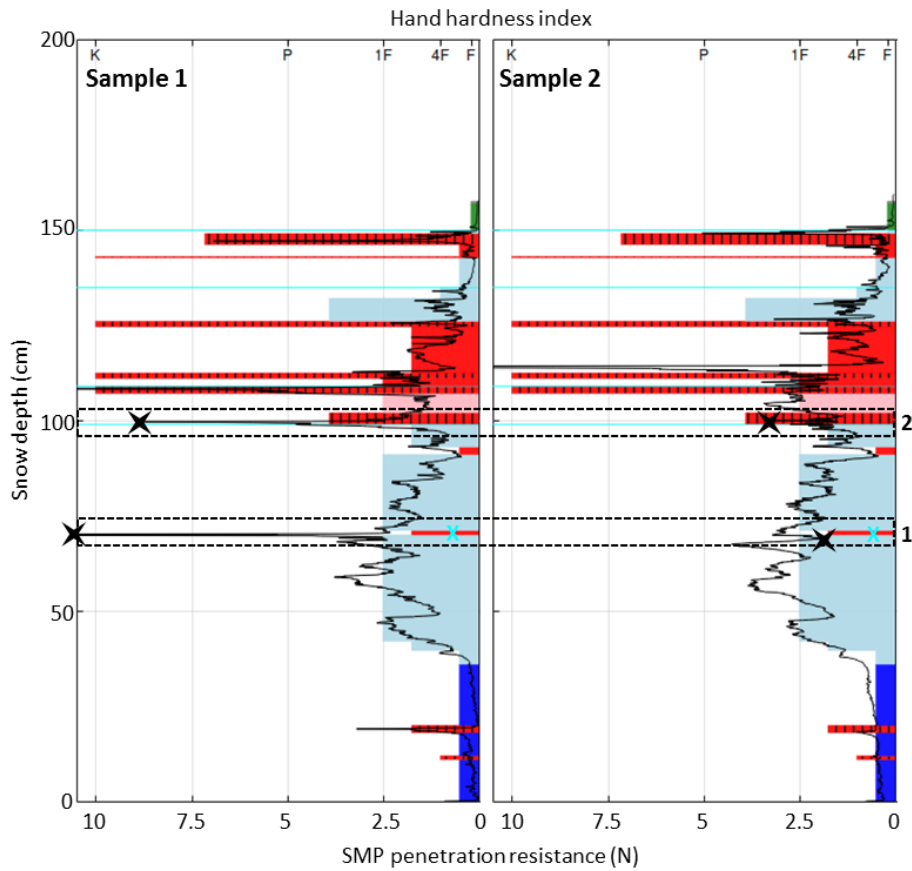


Figure 8. Two samples of SMP profiles of 4 April 2017 (black line), superimposed on the traditional snow profile of the same date. Colours referring to the grain shape and hand hardness index are defined accordingly to the classification of Fierz et al. (2009). Cyan crosses indicate ice lenses. Dashed rectangles highlight layers 1 and 2. Black crosses indicate the penetration resistance picked for each layer.

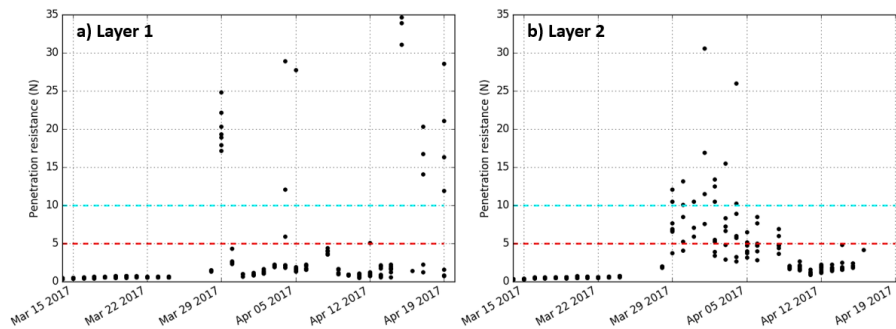


Figure 9. Evolution of the penetration resistance of a) layer 1 and b) layer 2, manually tracked in the SMP profiles, from 14 March to 19 April. Thresholds of 5 N and 10 N are indicated in red and cyan respectively, accordingly to Fig. 7.

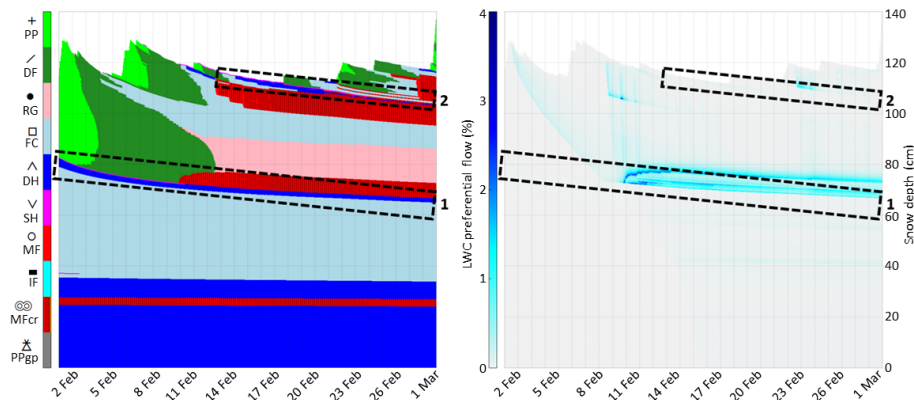


Figure 10. SNOWPACK simulation RE/PF, February 2017 at WFJ: a) grain shape, according to the classification of Fierz et al. (2009); b) liquid water content in the PF domain. Rectangles highlight layers 1 and 2.

3.2 Assessment of snowpack simulations

3.2.1 With different water transport schemes

240 Simulations of winter 2017 were first performed with the three water transport schemes existing in SNOWPACK (BA, RE and RE/PF). For the RE/PF simulation, Fig. 10 shows the grain shape and liquid water content in the PF domain for the month of February. Buried surface hoar of layer 1 (represented in fuchsia, at approximately 80 cm) is well simulated at the beginning of February. The capillary barrier of layer 2 is also well initiated in mid-February on the surface. However, a thick melt-freeze crust forms at layer 1 on 10 February (represented in hatched red, Fig. 10a). It is associated with some melting close to the surface leading to preferential water flow refreezing at capillary barrier of layer 1 (Fig. 10b). The water transferred for refreezing in the matrix domain is spread homogeneously which forms a crust with a density of approximately 320 kg m^{-3} . The transfer spreads vertically due to the issues mentioned in Sect. 2.2.2. This thick melt-freeze crust was not observed in the manual profiles nor the SMP measurements. Other melt-freeze crusts form close to the surface from mid-February. They were observed (Fig. 3) but were thinner than the simulated ones. A little surface melting is simulated on 1 February and leads to preferential flow (Fig. 10). Contrary to later simulated melting in mid-February, it was not observed: the measured snow surface temperature remained slightly under melting point. This simulation error is likely due to excessive surface turbulent fluxes input. New simulations were run without this melt water input, with no effect on the later snowpack structure due to the limited melting amount.

250 Figure 11 shows the grain shape and the liquid water content in the matrix domain from 15 March to 15 April, i.e. the period of transition from dry to ripe snowpack when ice layers formed (Sect. 3.1). No ice layer forms, except at the snowpack basis, which is probably due to a boundary effect at the interface between snow and soil. The thick melt-freeze crust is still present at layer 1, thus no ice layer forms (Fig. 11a). However, a higher water retention is simulated (Fig. 11b). Due to the excessive formation of melt-freeze crusts, the simulated snow microstructure at layer 2 does not reproduce the observed snow

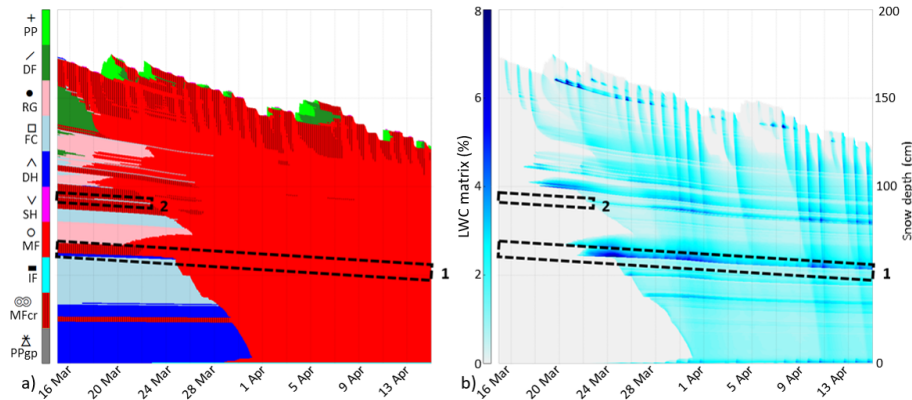


Figure 11. SNOWPACK simulation RE/PF, from 15 March to 15 April 2017 at WFJ: a) grain shape, according to the classification of Fierz et al. (2009); b) liquid water content in the matrix domain. Rectangles highlight layers 1 and 2.

microstructure and the capillary barrier, thus no ice layer forms. Matrix flow reaches the ground and the snowpack is entirely isothermal on 31 March (Fig. 11b), i.e. 9 days before the observations (Sect. 3.1.2). On 31 March, the water front was actually observed at around 100 cm (Fig. 4), hence a too early simulated water front progression.

A sensitivity study on the parameters of the dual-domain approach (Θ_{th} and N) was performed, but could not resolve the issues about ice formation highlighted here. Simulations were also analyzed in terms of snowpack runoff, confirming earlier findings (Wever et al., 2016; Würzer et al., 2017). The BA scheme underestimates the snowpack runoff, the RE scheme overestimates it, and the addition of preferential flow increases this overestimation (not shown). The onset of snowpack runoff is delayed compared to observations for BA and RE, because preferential flow is not simulated, but RE/PF simulations show the onset of snowpack runoff too early.

3.2.2 With ice reservoir parameterization

Simulations were also performed with the ice reservoir parameterization (RE/PF/IceR) to assess its ability to improve the simulation of ice layer formation compared to the previous simulations. Figure 12 shows the grain shape and liquid water content in the PF domain for the month of February. Similarly to the RE/PF simulation, the fine-over-coarse grain structure leads to water ponding in the PF domain at layer 1. But contrary to the RE/PF simulation, no melt-freeze crust forms at layer 1 (Fig. 12a): the water leaving the PF domain and refreezing is in too low quantity to be considered as representative of the mean state of the snowpack in this layer, it is thus stored in the ice reservoir. The fine-over-coarse grain transition forming a capillary barrier is preserved. Note that liquid water content in the PF domain (Fig. 12b) is almost not modified compared to the RE/PF simulation (Fig. 10b). Liquid water transport is similar, and in particular the vertical spreading of water ponding, but ice in the reservoir is concentrated at the capillary barrier. The ice kept in the reservoir has indeed no effect on water transport and microstructural changes in the matrix. At the end of February, less melt-freeze crusts are formed than in the RE/PF simulation, even though the ones surrounding layer 2 are also thicker than observed.

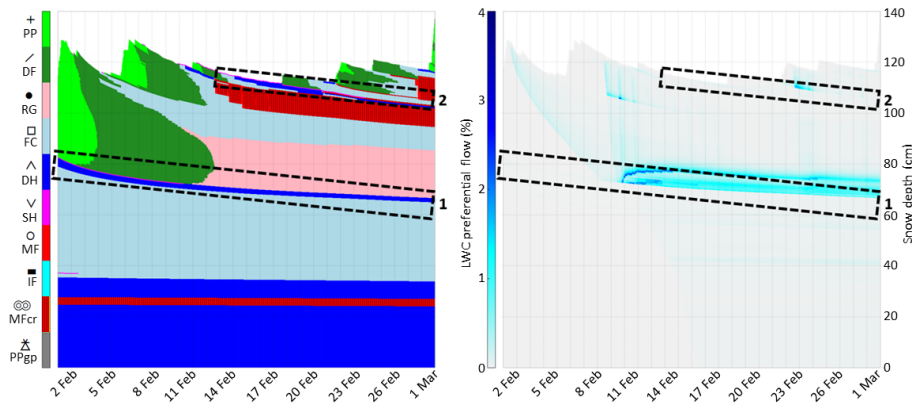


Figure 12. SNOwPACK simulation RE/PF/IceR, February 2017 at WFJ: a) grain shape, according to the classification of Fierz et al. (2009); b) liquid water content in the PF domain. Rectangles highlight layers 1 and 2.

280 Figure 13 shows the grain shape and the liquid water content in the matrix domain from 15 March to 15 April. A basal ice layer forms similarly to the RE/PF simulation. Contrary to the RE/PF simulation, the capillary barrier of layer 1 is still present (Fig. 13a). Melt forms appear at the layer transition from 22 March, and an ice layer forms in the matrix domain on 24 March, i.e. 4 to 5 days earlier than observed (Sect. 3.1.1 and Sect. 3.1.3). At this date, ice is transferred from the ice reservoir to the matrix domain (Fig. 14). The ice layer formed is 43 mm thick, with a dry density of 821 kg m^{-3} and a significant volumetric
 285 liquid water content of $\theta_{matrix} = 7.8\%$ and $\theta_{PF} = 1.7\%$ (on 24 March 13 UTC). Similarly to the RE/PF simulation, no ice forms at layer 2 due to the presence of melt-freeze crusts. However, less melt-freeze crusts are simulated in the snowpack, which is more in accordance with the observations. The matrix water flow reaches the ground on 30 March (Fig. 13b), i.e. 10 days before the observations (Sect. 3.1.2). The water front progression occurs too early, similarly to the RE/PF simulations. The ice reservoir does not modify the snowpack runoff compared to the RE/PF simulations (not shown).

290 3.2.3 Simulations over several winter seasons

To assess the impact of the ice reservoir parameterization on ice formation in the SNOwPACK model, simulations at WFJ are performed over 17 winters from 1999/2000 to 2015/2016, using the RE/PF and the RE/PF/IceR configurations. Only traditional snow profiles are available for evaluation, similarly to Wever et al. (2016). Ice layers at the snow-soil interface are not taken into account because of changing snowpack base in the observations over the winters (wooden board, gravel) and possible boundary
 295 effects in the simulations. Only simulated ice layers are verified against observations, to calculate hits (number of simulated ice layers matching an observation) and false alarms (number of simulated ice layers that do not match any observation). A height difference of 20 cm is used for matching of simulations and observations, similarly to Wever et al. (2016). We assume the formation date of an observed ice layer is comprised between the last snowpack profile without observed ice layer and the first profile where it is indicated. If the simulation date is more than one month away from the observed formation time interval,
 300 or if the height difference is more than 20 cm, the event is considered as a false alarm. Missed events (observed ice layers that

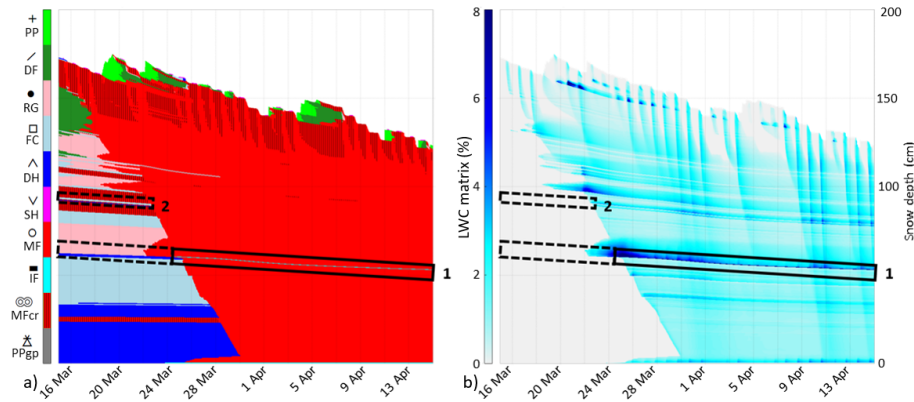


Figure 13. SNOWPACK simulation RE/PF/IceR, from 15 March to 15 April 2017 at WFJ: a) grain shape, according to the classification of Fierz et al. (2009); b) liquid water content in the matrix domain. Rectangles highlight layers 1 and 2, with dashed lines before ice formation in the matrix domain and solid lines afterwards.

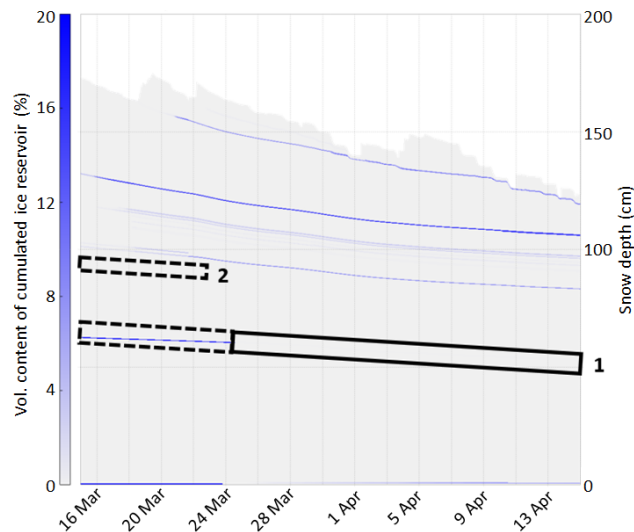


Figure 14. SNOWPACK simulation RE/PF/IceR, from 15 March to 15 April 2017 at WFJ: volumetric ice content in the cumulated ice reservoir. Rectangles highlight layers 1 and 2, with dashed lines before ice formation in the matrix domain and solid lines afterwards.

are not simulated) are not counted. Indeed, attributing fortnightly visual ice observations to a unique observed ice layer can be very ambiguous, contrary to simulated ice layers that persist in time. Results of this multi-year evaluation are summarized in Table 1.

Overall, the addition of the ice reservoir parameterization to the RE/PF scheme enables to form more ice layers, with a higher number of hits (15 against 6, with a one month tolerance) and a lower number of false alarms (1 against 6). The simulated ice formation date is in average 22 days earlier than the observation interval for the RE/PF scheme and 4 days earlier for the

Table 1. Hits (HI) and False Alarms (FA) of simulated ice layers for RE/PF and RE/PF/IceR simulations at WFJ, for 17 winter seasons, from 1999/2000 to 2015/2016. HI (height and date): simulated ice layers that match an observed one formed at less than 20 cm of height difference and in the same time interval. HI (height only): simulated ice layers that match an observed one formed at less than 20 cm of height difference and less than one month away from the observed time interval. FA: simulated but not observed ice layers (or more than one month away from the simulated formation).

	HI (height and date)	HI (height only)	FA
RE/PF	3	3	6
RE/PF/IceR	5	10	1

RE/PF/IceR scheme. The too early ice formation with the RE/PF scheme is consistent with the overestimation of simulated early season snowpack runoff from preferential flow as suggested by Wever et al. (2016). It is logically delayed in RE/PF/IceR simulations because the ice transits through the ice reservoir before being transferred to the matrix. The RE/PF/IceR configuration also mitigates the number of unobserved early melt-freeze crusts compared to the RE/PF configuration (not shown), as already highlighted for season 2016/2017 (Fig. 10 and Fig. 12). However, a very high number of ground ice layers were simulated (17 for the RE/PF/IceR scheme against 8 for the RE/PF scheme). This number is probably excessive, and due to possible snow-soil boundary effects.

4 Discussion

This detailed study of ice layer formation at Weissfluhjoch enables to assess both a comprehensive observation dataset and state-of-the-art 1D snowpack simulations for monitoring a complex process. We discuss hereafter the relevance of these methods and results.

First, the combined use of traditional snow profiles with measurements of higher temporal resolution like the SMP provides a suitable observation framework to study the transition period from dry to isothermal snowpack when ice formations appear due to preferential flow. Snowpack runoff measurements associated with snow temperature sensors and upGPR-derived water front gave insights about the homogeneous wetting of the snowpack and the period when the bottom of the snowpack was primarily affected by preferential flow. SMP profiles of penetration resistance showed clear signals of ice presence, when compared to visual observations, with values higher than 10 N (Fig. 7) while penetration resistances in dry snow were mostly lower than 2 N (Fig. 6) and melt-freeze crusts were characterized by intermediate penetration resistances (usually between 5 N and 10 N, Fig. 7). Identification of ice layers with several SMP profiles regularly spaced also offers a more quantitative estimate of ice heterogeneity than a subjective visual observation. However, the temporal and spatial variabilities may be complex to distinguish, as shown for layer 1 (Fig. 9). The visual layer tracking of SMP profiles is also a source of uncertainties. Hagenmuller and Pilloix (2016) developed a method matching several hardness profiles to synthesize them into one representative profile. This method was not considered relevant for the present study which focuses on local heterogeneity of ice layers. Moreover, when

330 ice layers are too thick, the SMP cannot go through them as happens often in spring. For winter 2017 at WFJ, no complete SMP
profile could be performed after 19 April. Finally, the difficulty to identify the exact date of ice formation or to attribute iso-
lated, fortnightly ice layer observations in traditional snowpack profiles to a unique ice layer (Sect. 3.2.3) highlights the added
value of the more comprehensive observation dataset used for winter 2016/2017. Overall, this comprehensive high-resolution
dataset (also including detailed measurements of density and specific surface area of the snow; Calonne et al., 2020) provides
335 valuable information for a thorough validation of today's and future snow cover models.

One-dimensional SNOWPACK simulations provide complementary insights to the observation dataset, despite the spatial
heterogeneity of ice layer formation due to preferential flow. The addition of an ice reservoir enables to parameterize the local
formation of ice at capillary barriers: it may thus be considered as representative of the volumetric content of ice lenses at a
given layer. These local specificities are not taken into account in the matrix domain, which is the mean state of the snowpack,
340 until they become homogeneously spread. This parameterization, which delays microstructural changes in the matrix due to
liquid water flow, is consistent with recent findings of Hirashima et al. (2019) who showed that preferential flow paths mi-
grate, thus gradually affecting the original snow microstructure. Several limitations may be noted. The matrix flow modeled
by Richards equation occurs too early and leads to an excessive snowpack runoff, which is even more enhanced by prefer-
ential flow. This may explain the too early formation of ice layer 1: the matrix water front reaches this level on 24 March in
345 simulations, while it is observed higher than 1 m on 24 March and the surrounding layers are still dry on 28 March in the
observations when the first ice lenses are observed. In addition, the performance of the RE/PF water transport scheme strongly
depends on a good representation of the snow microstructure by SNOWPACK, and particularly the grain radius and snow
density. For instance, no ice nor water ponding are simulated at layer 2 during winter 2017 because the observed capillary bar-
rier structure (rounded grains and faceted crystals above surface hoar) is not adequately represented (unobserved melt-freeze
350 crusts above layer 2). Finally, the implementation of the ice reservoir is meant to improve the representation of ice formation
within the 1D framework of the RE/PF dual-domain approach, but it does not mitigate the limitations of the preferential flow
parameterization. In particular, the vertical spreading of water flowing back from preferential to matrix domain is not solved:
its effect on ice formation is only mitigated with the cumulated ice reservoir. Advances in preferential water flow modelling in
the snowpack have recently been developed by Leroux and Pomeroy (2017, 2019) to tackle the capillary hysteresis effect and
355 capillary pressure overshoot. They could be considered to improve the representation of preferential flow in the SNOWPACK
model, through a more accurate determination of capillary pressure at the tip of the preferential flow path, with effects on the
water transfer from preferential flow to matrix domain.

Despite the limitations inherent to 1D simulation of preferential flow, the dual-domain approach combined to the ice reservoir
parameterization in SNOWPACK provides relevant information concerning deep ice layer formation. The ice reservoir limits
360 the formation of unobserved early melt-freeze crusts and, overall, enables to simulate more observed ice layers. For the detailed
study of winter 2017, it gives complementary insights on the formation of ice layer 1: according to the simulations, the vertical
preferential flow was sufficient to form the ice layer, even though a possible contribution of lateral flow cannot be totally
excluded.

5 Conclusions

365 We presented here a detailed study of deep ice layer formation in the snowpack due to preferential water flow at Weissfluhjoch, a high-altitude alpine site. Monitoring deep ice layers is of particular relevance for many applications, but is challenging in natural snow conditions. This research proposed an approach based on the combined use of a novel comprehensive observation dataset at high temporal resolution and detailed snow-cover modelling with improved ice formation representation.

Weekly traditional snow profiles, snowpack runoff and temperature measurements as well as upGPR-derived water front
370 height enabled to better monitor the dry-to-wet transition period between mid-March and mid-April 2017. In particular, the first days of measured snowpack runoff could be attributed to preferential water flow, and the exact date of first isothermal snowpack with matrix water flow reaching the ground could be identified. Daily penetration resistances measured with a SnowMicroPen (SMP) gave more accurate insights on ice layers, in complement to the traditional visual observations. Through comparisons with the visual observations, penetration resistance thresholds of 5 N and 10 N in SMP profiles could be defined
375 for the identification of melt-freeze crusts and ice layers, respectively. Ice formation could be monitored at higher temporal resolution, and the use of several profiles per day gave more quantitative information on ice spatial discontinuity. The daily succession of profiles also enabled to track the two main capillary barriers where ice formed, providing additional information on the evolution of the layers.

One-dimensional SNOWPACK simulations, including a parameterization of preferential flow, showed an overall good repre-
380 sentation of the snowpack structure, but a too early matrix wetting associated with an excessive snowpack runoff. The observed ice layers were not simulated due to the early formation of thick melt-freeze crusts, explained by limitations of the preferential flow scheme. We developed an ice reservoir parameterization to mitigate these limitations, with freezing water transferred from the preferential flow domain to an ice reservoir. The ice was included in the matrix domain when the layer could be considered to be continuous. This parameterization improved the simulation of winter 2017 with a limited number of unobserved early
385 melt-freeze crusts and the formation of one ice layer. However, the early transition to a wet snowpack was not improved, as the water transport was not modified. The ice reservoir scheme also showed improvements for the simulation of ice layers over past seasons.

These simulations highlighted the relevance of detailed snow-cover models for the modelling of complex phenomena like deep ice layers formed by preferential water flow, since an accurate representation of the snow microstructure is necessary.
390 Recent advances in preferential flow observations and modelling could contribute to strengthen water transport representation. This study also underlined the importance of comprehensive observation datasets for the validation of complex snow models. Collecting high-resolution data over more winter seasons will further improve the understanding of deep ice layer formation, particularly concerning their density, their impermeability and their evolution in the late melting season. Ice reservoir simulations also call for further experiments on large snowpack samples, similar to Yamaguchi et al. (2018), focusing on the formation
395 of discontinuous ice lenses due to preferential water flow.

Code and data availability. The dataset used in the paper will be available on the EnviDat database (doi will be provided). The ice reservoir parameterization for SNOWPACK will be available on models.slf.ch.

Author contributions. CF and AvH designed the study, carried out the field measurements and were responsible for the maintenance of the equipment. LQ was responsible for the modelling strategy, analyzed the measurements and simulations and wrote the manuscript. DL
400 processed the upGPR data to estimate the location of the water front. CF, AvH and NW helped to analyze measurements and simulations. All authors contributed to the manuscript.

Competing interests. The authors declare that the research was conducted in the absence of any commercial or financial relationships that could be construed as a potential conflict of interest.

Acknowledgements. We thank all the people from WSL Institute for Snow and Avalanche Research SLF involved in the measurements at
405 Weissfluhjoch. We would like to mention in particular Jean-Benoît Madore who helped out in the field during the dry-to wet transition of the snowpack.

References

- Albert, M. R. and Perron Jr., F. E.: Ice layer and surface crust permeability in a seasonal snow pack, *Hydrol. Process.*, 14, 3207–3214, [https://doi.org/10.1002/1099-1085\(20001230\)14:18<3207::AID-HYP196>3.0.CO;2-C](https://doi.org/10.1002/1099-1085(20001230)14:18<3207::AID-HYP196>3.0.CO;2-C), 2000.
- 410 Avanzi, F., Hirashima, H., Yamaguchi, S., Katsushima, T., and De Michele, C.: Observations of capillary barriers and preferential flow in layered snow during cold laboratory experiments, *The Cryosphere*, 10, 2013–2026, <https://doi.org/10.5194/tc-10-2013-2016>, 2016.
- Avanzi, F., Petrucci, G., Matzl, M., Schneebeli, M., and De Michele, C.: Early formation of preferential flow in a homogeneous snowpack observed by micro-CT, *Water Resour. Res.*, 53, 3713–3729, <https://doi.org/10.1002/2016WR019502>, 2017.
- Bartelt, P. and Lehning, M.: A physical SNOWPACK model for the Swiss avalanche warning: Part I: numerical model, *Cold Reg. Sci. Technol.*, 35, 123–145, [https://doi.org/10.1016/S0165-232X\(02\)00074-5](https://doi.org/10.1016/S0165-232X(02)00074-5), 2002.
- 415 Calonne, N., Geindreau, C., Flin, F., Morin, S., Lesaffre, B., Rolland du Roscoat, S., and Charrier, P.: 3-D image-based numerical computations of snow permeability: links to specific surface area, density, and microstructural anisotropy, *The Cryosphere*, 6, 939–951, <https://doi.org/10.5194/tc-6-939-2012>, 2012.
- Calonne, N., Richter, B., Löwe, H., Cetti, C., ter Schure, J., Van Herwijnen, A., Fierz, C., Jaggi, M., and Schneebeli, M.: The RHOSSA 420 campaign: multi-resolution monitoring of the seasonal evolution of the structure and mechanical stability of an alpine snowpack, *The Cryosphere*, 14, 1829–1848, <https://doi.org/10.5194/tc-14-1829-2020>, 2020.
- Coléou, C. and Lesaffre, B.: Irreducible water saturation in snow: experimental results in a cold laboratory, *Ann. Glaciol.*, 26, 64–68, <https://doi.org/10.3189/1998AoG26-1-64-68>, 1998.
- D’Amboise, C. J. L., Müller, K., Oxarango, L., Morin, S., and Schuler, T. V.: Implementation of a physically based water percolation routine 425 in the Crocus/SURFEX (V7.3) snowpack model, *Geosci. Model Dev.*, 10, 3547–3566, <https://doi.org/10.5194/gmd-10-3547-2017>, 2017.
- Denoth, A.: Snow dielectric measurements, *Adv. Space Res.*, 9, 233–243, [https://doi.org/10.1016/0273-1177\(89\)90491-2](https://doi.org/10.1016/0273-1177(89)90491-2), 1989.
- DiCarlo, D. A.: Capillary pressure overshoot as a function of imbibition flux and initial water content, *Water Resour. Res.*, 43, <https://doi.org/10.1029/2006WR005550>, 2007.
- DiCarlo, D. A.: Stability of gravity-driven multiphase flow in porous media: 40 Years of advancements, *Water Resour. Res.*, 49, 4531–4544, 430 <https://doi.org/10.1002/wrcr.20359>, 2013.
- Eiriksson, D., Whitson, M., Luce, C. H., Marshall, H. P., Bradford, J., Benner, S. G., Black, T., Hetrick, H., and McNamara, J. P.: An evaluation of the hydrologic relevance of lateral flow in snow at hillslope and catchment scales, *Hydrol. Process.*, 27, 640–654, <https://doi.org/10.1002/hyp.9666>, 2013.
- Fierz, C.: Temperature Profile of Snowpack, in: *Encyclopedia of Snow, Ice and Glaciers*, edited by Singh, V. P., Singh, P., and Haritashya, 435 U. K., pp. 1151–1154, Springer Netherlands, https://doi.org/10.1007/978-90-481-2642-2_569, 2011.
- Fierz, C., Armstrong, R. L., Durand, Y., Etchevers, P., Greene, E., McClung, D. M., Nishimura, K., Satyawali, P. K., and Sokratov, S. A.: The international classification for seasonal snow on the ground, IHP-VII Technical Documents in Hydrology No. 83, IACS Contribution No. 1, UNESCO-IHP, Paris, <http://unesdoc.unesco.org/images/0018/001864/186462e.pdf>, 2009.
- Hagenmuller, P. and Pilloix, T.: A New Method for Comparing and Matching Snow Profiles, Application for Profiles Measured by Penetrometers, *Front. Earth Sci.*, 4, 52, <https://doi.org/10.3389/feart.2016.00052>, 2016.
- 440 Hammonds, K. and Baker, I.: Investigating the thermophysical properties of the ice–snow interface under a controlled temperature gradient Part II: Analysis, *Cold Reg. Sci. Technol.*, 125, 12–20, <https://doi.org/10.1016/j.coldregions.2016.01.006>, 2016.

- Hammonds, K., Lieb-Lappen, R., Baker, I., and Wang, X.: Investigating the thermophysical properties of the ice–snow interface under a controlled temperature gradient: Part I: Experiments & Observations, *Cold Reg. Sci. Technol.*, 120, 157–167, 445 <https://doi.org/10.1016/j.coldregions.2015.09.006>, 2015.
- Hirashima, H., Yamaguchi, S., and Katsushima, T.: A multi-dimensional water transport model to reproduce preferential flow in the snowpack, *Cold Reg. Sci. Technol.*, 108, 80–90, <https://doi.org/10.1016/j.coldregions.2014.09.004>, 2014.
- Hirashima, H., Avanzi, F., and Yamaguchi, S.: Liquid water infiltration into a layered snowpack: evaluation of a 3-D water transport model with laboratory experiments, *Hydrol. Earth Syst. Sci.*, 21, 5503–5515, <https://doi.org/10.5194/hess-21-5503-2017>, 2017.
- 450 Hirashima, H., Avanzi, F., and Wever, N.: Wet-snow metamorphism drives the transition from preferential to matrix flow in snow, *Geophys. Res. Lett.*, 46, <https://doi.org/10.1029/2019GL084152>, 2019.
- Jamieson, B.: Formation of refrozen snowpack layers and their role in slab avalanche release, *Rev. Geophys.*, 44, <https://doi.org/10.1029/2005RG000176>, RG2001, 2006.
- Juras, R., Würzer, S., Pavlásek, J., Vitvar, T., and Jonas, T.: Rainwater propagation through snowpack during rain-on-snow sprinkling experiments under different snow conditions, *Hydrol. Earth Syst. Sci.*, 21, 4973–4987, <https://doi.org/10.5194/hess-21-4973-2017>, 2017.
- 455 Katsushima, T., Yamaguchi, S., Kumakura, T., and Sato, A.: Experimental analysis of preferential flow in dry snowpack, *Cold Reg. Sci. Technol.*, 85, 206–216, <https://doi.org/10.1016/j.coldregions.2012.09.012>, 2013.
- Katsushima, T., Adachi, S., Yamaguchi, S., Ozeki, T., and Kumakura, T.: Observation of fingering flow and lateral flow development in layered dry snowpack by using MRI, in: *International Snow Science Workshop Proceedings 2018*, Innsbruck, Austria, pp. 971–975, 460 <http://arc.lib.montana.edu/snow-science/item/2689>, 2018.
- Katsushima, T., Adachi, S., Yamaguchi, S., Ozeki, T., and Kumakura, T.: Nondestructive three-dimensional observations of flow finger and lateral flow development in dry snow using magnetic resonance imaging, *Cold Reg. Sci. Technol.*, 170, 102956, <https://doi.org/10.1016/j.coldregions.2019.102956>, 2020.
- Larue, F., Royer, A., De Sève, D., Roy, A., Picard, G., Vionnet, V., and Cosme, E.: Simulation and Assimilation of Passive Microwave 465 Data Using a Snowpack Model Coupled to a Calibrated Radiative Transfer Model Over Northeastern Canada, *Water Resour. Res.*, 54, 4823–4848, <https://doi.org/10.1029/2017WR022132>, 2018.
- Leroux, N. R. and Pomeroy, J. W.: Modelling capillary hysteresis effects on preferential flow through melting and cold layered snowpacks, *Adv. Water Resour.*, 107, 250–264, <https://doi.org/10.1016/j.advwatres.2017.06.024>, 2017.
- Leroux, N. R. and Pomeroy, J. W.: Simulation of Capillary Pressure Overshoot in Snow Combining Trapping of the Wetting Phase With a 470 Nonequilibrium Richards Equation Model, *Water Resour. Res.*, 55, 236–248, <https://doi.org/10.1029/2018WR022969>, 2019.
- Machguth, H., MacFerrin, M., van As, D., Box, J. E., Charalampidis, C., Colgan, W., Fausto, R. S., Meijer, H. A. J., Mosley-Thompson, E., and van de Wal, R. S. W.: Greenland meltwater storage in firn limited by near-surface ice formation, *Nat. Clim. Change*, 6, 390–393, <https://doi.org/10.1038/nclimate2899>, 2016.
- Marsh, P.: Water Flow through Snow and Firn, in: *Encyclopedia of Hydrological Sciences*, edited by Anderson, M. G. and McDonnell, J. J., 475 <https://doi.org/10.1002/0470848944.hsa167>, 2006.
- Marty, C. and Meister, R.: Long-term snow and weather observations at Weissfluhjoch and its relation to other high-altitude observatories in the Alps, *Theor. Appl. Climatol.*, 110, 573–583, <https://doi.org/10.1007/s00704-012-0584-3>, 2012.
- Mualem, Y.: A new model for predicting the hydraulic conductivity of unsaturated porous media, *Water Resour. Res.*, 12, 513–522, <https://doi.org/10.1029/WR012i003p00513>, 1976.

- 480 Ozeki, T. and Akitaya, E.: Energy balance and formation of sun crust in snow, *Ann. Glaciol.*, 26, 35–38, <https://doi.org/10.3189/1998AoG26-1-35-38>, 1998.
- Pfeffer, W. T. and Humphrey, N. F.: Formation of ice layers by infiltration and refreezing of meltwater, *Ann. Glaciol.*, 26, 83–91, <https://doi.org/10.1017/S0260305500014610>, 1998.
- Quéno, L., Vionnet, V., Cabot, F., Vrécourt, D., and Dombrowski-Etchevers, I.: Forecasting and modelling ice layer formation on the snow-
485 pack due to freezing precipitation in the Pyrenees, *Cold Reg. Sci. Technol.*, 146, 19–31, <https://doi.org/10.1016/j.coldregions.2017.11.007>, 2018.
- Rees, A., Lemmetyinen, J., Derksen, C., Pulliainen, J., and English, M.: Observed and modelled effects of ice lens formation on passive microwave brightness temperatures over snow covered tundra, *Remote Sens. Environ.*, 114, 116–126, <https://doi.org/10.1016/j.rse.2009.08.013>, 2010.
- 490 Reynolds, J. M.: *An introduction to applied and environmental geophysics*, John Wiley & Sons, 2011.
- Richter, B., Schweizer, J., Rotach, M. W., and van Herwijnen, A.: Validating modeled critical crack length for crack propagation in the snow cover model SNOWPACK, *The Cryosphere*, 13, 3353–3366, <https://doi.org/10.5194/tc-13-3353-2019>, 2019.
- Roy, A., Royer, A., St-Jean-Rondeau, O., Montpetit, B., Picard, G., Mavrovic, A., Marchand, N., and Langlois, A.: Microwave snow emission modeling uncertainties in boreal and subarctic environments, *The Cryosphere*, 10, 623–638, <https://doi.org/10.5194/tc-10-623-2016>, 2016.
- 495 Sand, K. and Bruland, O.: Application of Georadar for Snow Cover Surveying, *Hydrol. Res.*, 29, 361–370, <https://doi.org/10.2166/nh.1998.0026>, 1998.
- Schmid, L., Heilig, A., Mitterer, C., Schweizer, J., Maurer, H., Okorn, R., and Eisen, O.: Continuous snowpack monitoring using upward-looking ground-penetrating radar technology, *J. Glaciol.*, 60, 509–525, <https://doi.org/10.3189/2014JG13J084>, 2014.
- Schneebeli, M.: Development and stability of preferential flow paths in a layered snowpack, in: *Biogeochemistry of Seasonally Snow-Covered Catchments (Proceedings of a Boulder Symposium July 1995)*, edited by Tonnessen, K., Williams, M., and Tranter, M., vol. 228, pp. 89–95, IAHS, 1995.
- 500 Schneebeli, M., Pielmeier, C., and Johnson, J. B.: Measuring snow microstructure and hardness using a high resolution penetrometer, *Cold Reg. Sci. Technol.*, 30, 101–114, [https://doi.org/10.1016/S0165-232X\(99\)00030-0](https://doi.org/10.1016/S0165-232X(99)00030-0), 1999.
- Singh, P., Spitzbart, G., Huebl, H., and Weinmeister, H. W.: Importance of ice layers on liquid water storage within a snowpack, *Hydrol. Process.*, 13, 1799–1805, [https://doi.org/10.1002/\(SICI\)1099-1085\(199909\)13:12/13<1799::AID-HYP880>3.0.CO;2-M](https://doi.org/10.1002/(SICI)1099-1085(199909)13:12/13<1799::AID-HYP880>3.0.CO;2-M), 1999.
- van Genuchten, M. T.: A closed-form equation for predicting the hydraulic conductivity of unsaturated soils, *Soil Sci. Soc. Am. J.*, 44, 892–898, <https://doi.org/10.2136/sssaj1980.03615995004400050002x>, 1980.
- Vionnet, V., Brun, E., Morin, S., Boone, A., Faroux, S., Le Moigne, P., Martin, E., and Willemet, J.-M.: The detailed snowpack scheme Crocus and its implementation in SURFEX v7.2, *Geosci. Model Dev.*, 5, 773–791, <https://doi.org/10.5194/gmd-5-773-2012>, 2012.
- 510 Watts, T., Rutter, N., Toose, P., Derksen, C., Sandells, M., and Woodward, J.: Brief communication: Improved measurement of ice layer density in seasonal snowpacks, *The Cryosphere*, 10, 2069–2074, <https://doi.org/10.5194/tc-10-2069-2016>, 2016.
- Webb, R. W., Fassnacht, S. R., Gooseff, M. N., and Webb, S. W.: The Presence of Hydraulic Barriers in Layered Snowpacks: TOUGH2 Simulations and Estimated Diversion Lengths, *Transport Porous Med.*, 123, 457–476, <https://doi.org/10.1007/s11242-018-1079-1>, 2018a.
- Webb, R. W., Williams, M. W., and Erickson, T. A.: The Spatial and Temporal Variability of Meltwater Flow Paths: Insights From a Grid of
515 Over 100 Snow Lysimeters, *Water Resour. Res.*, 54, 1146–1160, <https://doi.org/10.1002/2017WR020866>, 2018b.
- Wever, N., Fierz, C., Mitterer, C., Hirashima, H., and Lehning, M.: Solving Richards Equation for snow improves snowpack meltwater runoff estimations in detailed multi-layer snowpack model, *The Cryosphere*, 8, 257–274, <https://doi.org/10.5194/tc-8-257-2014>, 2014.

- Wever, N., Schmid, L., Heilig, A., Eisen, O., Fierz, C., and Lehning, M.: Verification of the multi-layer SNOWPACK model with different water transport schemes, *The Cryosphere*, 9, 2271–2293, <https://doi.org/10.5194/tc-9-2271-2015>, 2015.
- 520 Wever, N., Würzer, S., Fierz, C., and Lehning, M.: Simulating ice layer formation under the presence of preferential flow in layered snowpacks, *The Cryosphere*, 10, 2731–2744, <https://doi.org/10.5194/tc-10-2731-2016>, 2016.
- WSL Institute for Snow and Avalanche Research SLF: WFJ_MOD: Meteorological and snowpack measurements from Weissfluhjoch, Davos, Switzerland, <https://doi.org/10.16904/1>, 2015.
- Würzer, S., Wever, N., Juras, R., Lehning, M., and Jonas, T.: Modelling liquid water transport in snow under rain-on-snow conditions –
525 considering preferential flow, *Hydrol. Earth Syst. Sci.*, 21, 1741–1756, <https://doi.org/10.5194/hess-21-1741-2017>, 2017.
- Yamaguchi, S., Watanabe, K., Katsushima, T., Sato, A., and Kumakura, T.: Dependence of the water retention curve of snow on snow characteristics, *Ann. Glaciol.*, 53, 6–12, <https://doi.org/10.3189/2012AoG61A001>, 2012.
- Yamaguchi, S., Hirashima, H., and Ishii, Y.: Year-to-year changes in preferential flow development in a seasonal snowpack and their dependence on snowpack conditions, *Cold Reg. Sci. Technol.*, 149, 95–105, <https://doi.org/10.1016/j.coldregions.2018.02.009>, 2018.